The androgen receptor in mesenchymal progenitors regulates skeletal muscle mass via *Igf1* expression in male mice.

Hiroshi Sakai[1,2,*], Hideaki Uno[2], Harumi Yamakawa[2], Kaori Tanaka[3], Aoi Ikedo[1], Akiyoshi Uezumi[4], Yasuyuki Ohkawa[3], Yuuki Imai[1,2,*]

[1]Division of Integrative Pathophysiology, Proteo-Science Center, Ehime University, Toon, Ehime 791-0295, Japan.

[2]Department of Pathophysiology, Ehime University Graduate School of Medicine, Toon, Ehime 791-0295, Japan.

[3]Division of Transcriptomics, Medical Institute of Bioregulation, Kyushu University, Higashi-ku, Fukuoka 812-0054, Japan.

[4]Divison of Cell Heterogeneity, Medical Institute of Bioregulation, Kyushu University, Higashi-ku, Fukuoka 812-0054, Japan.

Keywords

Androgen receptor, skeletal muscle, mesenchymal progenitors, Igf1

[*]Correspondence

sakai.hiroshi.wh@ehime-u.ac.jp (H.S.), y-imai@m.ehime-u.ac.jp (Y.I.)

Reprint requests

Hiroshi Sakai, DVM, PhD, or Yuuki Imai, MD, PhD, Proteo-Science Center, Graduate School of Medicine, Ehime University, Shitsukawa, Toon, Ehime, 791-0295, Japan.

Funding

This work was supported in part by MEXT/JSPS KAKENHI (JP21K17568 to H.S.; JP22H03203 to Y.I.) and the HIRAKU-Global Program, which is funded by MEXT's "Strategic Professional Development Program for Young Researchers" (to H.S.).

Declaration of interest

The authors declare no competing interests.

Abstract

Androgens exert their effects primarily by binding to the androgen receptor (AR), a ligand-dependent nuclear receptor. While androgens have anabolic effects on skeletal muscle, previous studies reported that AR functions in myofibers to regulate skeletal muscle quality, rather than skeletal muscle mass. Therefore, the anabolic effects of androgens are exerted via extra-myofiber cells or tissues. In this context, the cellular and molecular mechanisms of AR in mesenchymal progenitors, which play a crucial role in maintaining skeletal muscle homeostasis, remain largely unknown. In this study, we demonstrated expression of AR in mesenchymal progenitors and found that targeted AR ablation in mesenchymal progenitors reduced limb muscle mass in mature adult, but not young or aged, male mice, although fatty infiltration of muscle was not affected. The absence of AR in mesenchymal progenitors led to remarkable perineal muscle hypotrophy, regardless of age, due to abnormal regulation of transcripts associated with apoptosis and proteolysis. Additionally, we revealed that AR in mesenchymal progenitors regulates the expression of insulin-like growth factor 1, which can increase skeletal muscle mass in a paracrine manner. These findings indicate that the anabolic effects of androgens indirectly regulate skeletal muscle mass via, at least in part, AR signaling in mesenchymal progenitors.

Introduction

Androgens are crucial regulators of various biological processes, including the development and maintenance of male characteristics. Notably, in a physiological context, the administration of androgens or androgen analogs has been shown to exert anabolic effects on muscles, resulting in increased muscle mass, strength, and body weight (1,2). These physiological effects are mediated by activation of the androgen receptor (AR), a member of the nuclear receptor superfamily (3). However, despite that clinical administration of androgens in men can successfully increase skeletal muscle mass (4), the precise cellular and molecular mechanisms underlying the function of AR in muscle remain largely unexplored.

Skeletal muscle represents a complex tissue comprising multiple cell types, and the effects of androgens are likely mediated by various cell populations expressing AR within skeletal muscles. While male mice systemically lacking AR exhibit low skeletal muscle strength and mass, similar to female levels (5), we previously showed that muscle hypertrophy can be induced by androgen administration even in the absence of AR in muscle fibers, suggesting that non-myofiber AR contributes to the regulation of muscle mass (6). Furthermore, another of our studies demonstrated that deletion of AR in satellite cells, which are muscle stem cells responsible for muscle regeneration, had a limited effect on their proliferation and differentiation (7). Additionally, since limb muscle mass remains unaffected even in mice with AR ablation in both myofibers and muscle stem cells (8), other cells expressing AR within the muscles may play a role in regulating skeletal muscle mass.

Mesenchymal progenitors (9), also known as fibro/adipogenic progenitors (10), have been identified as a cell population distinct from myogenic cells characterized by the expression of platelet-derived growth factor receptor alpha (PDGFRα). These cells are involved in the

maintenance and regeneration of skeletal muscle (11,12). Conversely, mesenchymal progenitors have been implicated in pathological fibrosis and fat accumulation in skeletal muscle (13). AR expression has been reported in cells located in the interstitium or outside the basal lamina in both mouse and human skeletal muscles (14,15). Additionally, ablation of AR specifically in embryonic cells of the mesenchyme led to impaired development of the perineal levator ani (LA) and bulbocavernosus (BC) muscles (16), which are particularly responsive to androgen. Furthermore, the reduced proliferation of undifferentiated myoblasts in these mutant mice suggested a potential paracrine regulatory role of mesenchymal AR in controlling skeletal muscles (16). Despite this knowledge, the specific role of AR in adult mesenchymal progenitors in skeletal muscles remains unexplored.

Here we investigate the role of AR expressed in mesenchymal progenitors in muscle maintenance using mice with mesenchymal progenitor-specific AR ablation. We show that AR in mesenchymal progenitors plays a critical role in maintaining skeletal muscle mass via regulation of insulin-like growth factor 1 (Igf1) expression in male mice.

Materials and Methods

Animals

PDGFRα-CreER mice (17) and *HSA-Cre*$^{Tg/+}$ mice (18) were purchased from Jackson Laboratories (Strain #: 018280 and 006149). *AR*$^{L2/Y}$ mice have been described previously (19). *PDGFRα-CreER* male mice were crossed with *AR*$^{L2/+}$ female mice to generate *PDGFRα-CreER;AR*$^{L2/Y}$ male mutant mice. Male littermates with the *PDGFRα-CreER;AR*$^{+/Y}$ genotype were used as control mice. To generate *HSA-Cre*$^{Tg/+}$*;PDGFRα-CreER;AR*$^{L2/Y}$ male mice, *HSA-Cre*$^{Tg/+}$ male mice were crossed with *PDGFRα-CreER;AR*$^{L2/+}$ female mice. All mice were housed in a specific pathogen-free facility under climate-controlled conditions and a 12-h light/dark cycle and were provided water and a standard diet *ad libitum*. In both control and mutant mice, 100 µL 20 mg/mL tamoxifen (Sigma-Aldrich, Cat# T5648), dissolved in corn oil (Sigma-Aldrich, Cat# C8267), was injected intraperitoneally for 5 consecutive days at 8 or 12 weeks of age. A high-fat diet (HFD, CLEA Japan, Cat# HFD32) was given *ad libitum* for 8 weeks to induce obesity in mice. The diet was refreshed every 2 days. To induce fatty infiltration of skeletal muscle, 100 µL 50% v/v glycerol was injected into tibialis anterior (TA) muscles under anesthesia using isoflurane (20). To induce AR signaling, dihydrotestosterone (DHT or stanolone, 2.5 mg/mouse; Tokyo Chemical Industry, Cat# A0462), dissolved in absolute ethanol and diluted in 0.3% w/v hydroxypropyl cellulose (Wako, Cat# 085-07932) in PBS, was injected subcutaneously at 2 hours before sampling. All animal experiments were approved by the Animal Experiment Committee of Ehime University (Approval No. 37A1-1·16) and were conducted in full compliance with the Guidelines for Animal Experiments at Ehime University.

Grip strength

The grip strength of the forelimb was measured using a strain gauge (Melquest, Cat# GPM-100B). The maximal force was determined after 10 measurements. The mean value recorded by two independent experimenters was reported as the grip strength of each mouse.

Immunofluorescence staining and microscopy

For immunofluorescence staining, muscles were snap frozen in liquid nitrogen-chilled isopentane. Cryosections of 10 μm thickness were prepared for immunofluorescence staining. Sections were fixed in 4% paraformaldehyde in PBS for 5 min, blocked in 5% goat serum (Gibco, Cat# 16210-064) in PBS for 60 min, and incubated with primary antibodies overnight at 4°C. For staining of myosin heavy chain (Myh), sections were air-dried and blocked with M.O.M. reagent (Vector Laboratories, Cat# MKB-2213-1) at room temperature for 60 min. Primary antibodies for Myh diluted in 1% BSA/PBS were incubated at 37°C for 45 min. The antibodies used for immunofluorescence staining were anti-Pax7 (DSHB, Cat# PAX7, RRID:AB_528428; 1/5 dilution), anti-PDGFRA (R&D Systems, Cat# AF1062, RRID:AB_2236897; 1/80), anti-AR (Abcam, Cat# ab108341, RRID:AB_10865716; 1/100), anti-Laminin α2 (Santa Cruz Biotechnology, Cat# sc-59854, RRID:AB_784266; 1/400), anti-Laminin (Sigma-Aldrich, Cat# L9393, RRID:AB_477163; 1/500), anti-Myh7 (DSHB, Cat# BA-D5, RRID:AB_2235587, supernatant; 1/100), anti-Myh2 (DSHB, Cat# SC-71, RRID:AB_2147165, supernatant; 1/100), anti-Myh4 (DSHB, Cat# BF-F3, RRID:AB_2266724, concentrated purified; 1/100), anti-Perilipin (Sigma-Aldrich, Cat# P1873, RRID:AB_532267; 1/250), Alexa fluor 568 goat anti-mouse IgG1 (Thermo Fisher Scientific, Cat# A-21124; RRID: AB_2535766; 1/1000), Alexa fluor 488 goat anti-rabbit IgG (Thermo Fisher Scientific, Cat# A-11008; RRID:AB_143165; 1/1000), Alexa fluor 488 goat anti-mouse IgM (Thermo Fisher

Scientific, Cat# A-21042; RRID:AB_143165; 1/1000), and Alexa fluor 647 goat anti-rabbit IgG (Thermo Fisher Scientific, Cat# A27040; RRID:AB_143165; 1/1000). Nuclei were counterstained with DAPI.

Quantification of muscle sections

Entire cross sections of fluorescence images stained with laminin and Myh were photographed using BIOREVO (Keyence) or Axio Observer7 (Zeiss). To quantify the number, cross-sectional area (CSA), and minimal Ferret diameter of the myofibers, captured images were analyzed using Fiji (v2.3.0) (https://imagej.net/Fiji). The myofiber area was identified by the laminin+ signals. The region of interest was set within the laminin+ areas. The frequency of each fiber type in the region of interest was recorded by Trainable Weka Segmentation in Fiji after manual training. Small (< 150 μm^2) or large (> 10,000 μm^2) fibers were excluded for analyzing. To quantify perilipin+ adipocytes, the perilipin+ area was manually measured using Fiji.

Isolation of mesenchymal progenitors from skeletal muscle

Isolation of mononuclear cells from muscle was performed as described previously (21) with minor modifications. Briefly, muscles were chopped in PBS on ice and digested using 800 U/mL collagenase type 2 (Worthington, Cat# LS004177) in F10 medium (Gibco, Cat# 11550-043) supplemented with 10% horse serum (Gibco, Cat# 26050-088) and antibiotic–antimycotic (Gibco, Cat# 15240-062) for 60 min. Another digestion was conducted using 1000 U/mL collagenase type 2 and 11 U/mL dispase (Gibco, Cat# 17105-041) for 30 min. The supernatants were transferred to a cell strainer (Falcon, Cat# 352340) to filter the debris and then centrifuged to yield a cell suspension. The following antibodies were used: CD31-FITC (BioLegend, Cat#

102406; RRID:AB_312901; 1/100 dilution), CD45-FITC (BioLegend, Cat# 103108, RRID:AB_312973; 1/100 dilution), Vcam1-PE (Thermo Fisher Scientific, Cat# 12-1061-82, RRID:AB_2572573; 1/100 dilution), and PDGFRA-APC (R&D Systems, Cat# FAB1062A, RRID:AB_3073817; 1/30 dilution). The BD FACSAria II (RRID:SCR_018091) or BD FACSAria Fusion (BD Biosciences) was used for fluorescence-activated cell sorting of the cells, and the plot was analyzed by FlowJo v10.1r7 (BD Life Sciences, RRID:SCR_008520).

RNA-seq and data analysis

For isolation of RNA from mesenchymal progenitors in LA/BC muscles, 300 PDGFRα+ cells were sorted into the wells of a 96-well plate containing 10 µL lysis buffer at 4°C. The lysis buffer was prepared by mixing 1 µL RNase inhibitor (TaKaRa, Cat# 2313A) and 19 µL 10X lysis buffer (TaKaRa, Cat# 635013) diluted to 1X with nuclease-free water. 3' UTR RNA-seq was conducted using the CEL-Seq2 protocol (22), with the exception of employing the Second Strand Synthesis Module (NEB) for double-stranded cDNA synthesis. The library was then amplified via 10 cycles of PCR without any sample pooling. Subsequently, the library was sequenced on the Illumina NovaSeq6000, and quantitative analysis was performed using 81 bp of insert reads (Read2).

Cell barcode and UMI information from Read1 were extracted using UMI-tools (v1.1.2) (23) with the following command: “umi_tools extract -I read1.fastq --read2-in=read2.fastq --bc-pattern=NNNNNNNNNNCCCCCCCC”. Adaptor and low-quality sequences were removed, and reads with a length less than 20 bp were discarded using TrimGalore (v0.6.7; http://www.bioinformatics.babraham.ac.uk/projects/trim_galore/). The processed reads were then mapped to the GRCm38 reference genome using HISAT2 (v2.2.1) (24). Read counts for each

gene were obtained using featureCounts (v2.0.1) (25), and UMI duplications were removed using UMI-tools. Four cell barcodes, "ATGCAATGC," "GACACGACA," "CGATGCGAT," and "TCTGGTCTG," were assigned to each sample. Differentially expressed genes were identified using DESeq2 (v1.36.0) (26) with thresholds of $|\log2FC| > 1$ and $padj < 0.1$. Metascape (27) was used for Gene Ontology enrichment analysis.

RNA isolation and quantitative real-time PCR

Total RNA was extracted from freshly sorted 30,000 PDGFRα+ cells from LA/BC muscles using the RNeasy Plus Micro Kit (Qiagen, Cat# 74034) following the manufacturer's protocol. Reverse transcription was performed using PrimeScript (Takara, Cat# RR036A) to synthesize cDNA from total RNA. Quantitative PCR (qPCR) was conducted in duplicate samples utilizing TB Green Premix Ex Taq II (Takara, Cat# RR820S) and the Thermal Cycler Dice (Takara, Cat# TP850). The expression levels of the target genes were normalized to that of Rpl13a. The primer sequences are listed in Table 1.

Statistical analysis

Prism 9 (GraphPad Software) or R (v4.0.5) (https://www.r-project.org) was used for the statistical analysis. Welch's t-test was used to compare two groups. To compare variables among three or more groups, Welch's ANOVA with Dunnett's T3 multiple comparison test was used.

Results

AR ablation in mesenchymal progenitors was validated in *PDGFRα-CreER;AR*$^{L2/Y}$ mice

AR expression in fibroblasts of the perineal muscle LA and in mesenchymal cells of the fetal LA has been reported (14,16,28); however, it is unknown whether mesenchymal progenitors in adult limb muscle express AR. To examine the expression pattern of AR in mesenchymal progenitors, immunofluorescence staining of PDGFRα, a marker of mesenchymal progenitors (9), and AR was performed in adult male mice. We found that AR was expressed in mesenchymal progenitors staining positive for PDGFRα (Fig. 1A), as well as in muscle fibers surrounded by laminin-expressing basal lamina, consistent with previous findings (28,29).

To investigate the role of AR in mesenchymal progenitors, *PDGFRα-CreER* (17) and *AR*$^{L2/Y}$ (19) mice were crossed to selectively delete the AR gene in mesenchymal progenitors expressing PDGFRα. Tamoxifen (TMX) was administered to Cre control male mice (*PDGFRα-CreER*) and mutant male mice (*PDGFRα-CreER;AR*$^{L2/Y}$) for 5 consecutive days to induce AR ablation (Fig. 1B). To assess the efficiency of AR ablation, immunofluorescence staining of PDGFRα and AR was performed in Cre control and mutant mice. Quantification of PDGFRα and AR expression in forelimb biceps brachii (BB) and hindlimb TA muscles demonstrated a significant decrease of 90% in AR protein in mutant mice compared with Cre control mice, confirming successful ablation of AR expression in mesenchymal progenitors from *PDGFRα-CreER;AR*$^{L2/Y}$ mice (Fig. 1C). In contrast, loss of AR in mesenchymal progenitors did not affect the number of PDGFRα+ cells (Fig. 1D). Taken together, these findings demonstrate successful and specific loss of AR expression in PDGFRα+ cells, rendering them an optimal model for investigating AR in mesenchymal progenitors in skeletal muscles.

Lack of AR in mesenchymal progenitors had a limited effect on steady-state limb skeletal muscles

Because ablation of PDGFRα+ cells in intact muscles results in skeletal muscle atrophy (11,12), we first analyzed the muscles of Cre control and mutant mice under steady-state conditions at a young age (14 weeks) (Fig. 2A). Body weight and limb skeletal muscle mass were not affected in mutant compared with control mice at 2 weeks after TMX administration (Fig. 2B). Moreover, the grip strength of mutant mice was comparable with that of control mice (Fig. 2C). The minimal Ferret diameter and number of myofibers in BB and TA muscles remained unchanged in mutant mice (Fig. 2D, E). As relayed signaling between mesenchymal progenitors and muscle stem (satellite) cells is critical for muscle hypertrophy (30), we also quantified the number of muscle stem cells. Staining of Pax7, a marker of muscle stem cells (31), revealed no difference in the number of muscle stem cells between control and mutant BB and TA muscles (Fig. 2F). We next investigated the fiber types of slow soleus muscles, which are affected by muscle fiber- and muscle stem cell-specific AR ablation (8,32). Analysis of soleus muscles fiber types by immunofluorescence staining of type I (Myh7), type IIa (Myh2), and type IIx/IIb (without signals) muscle fibers demonstrated no difference in the fiber-type parameters (minimal Ferret diameter and frequency of each fiber-type) between control and mutant mice (Fig. 2G, H). Thus, AR expression loss in mesenchymal progenitors has a limited effect on the steady-state limb muscles of young mice.

The impact of AR deficiency in mesenchymal progenitors on adipogenesis in muscles was limited

We also examined the adipogenesis of mesenchymal progenitors in mutant mice because adipocytes originate from mesenchymal progenitors in skeletal muscles (9). In mice, the presence of adipocytes in skeletal muscle is typically uncommon. To address this, we employed two models: administration of a HFD to the mice and a muscle injury model utilizing glycerol injection in the mice. First, both the control and mutant mice were subjected to an 8-week regimen of HFD feeding (Fig. 3A). No significant differences were observed between the mutant mice and control mice in terms of total body weight, hindlimb muscle weights, epididymal white adipose tissue mass (eWAT), and subcutaneous white adipose tissue (sWAT) mass (Fig. 3B), and grip strength (Fig. 3C). Immunofluorescence staining of perilipin, a marker of adipocytes (33), along with laminin, demonstrated no significant difference in the minimal Ferret diameter of myofibers or the area occupied by adipocytes between the control and mutant TA muscles (Fig. 3D, E).

To further investigate the impact of AR deficiency in muscle adipogenesis, we employed a muscle injury model by administering glycerol injections into the TA muscle of both control and mutant mice (Fig. 3F). No significant differences were observed between the control and mutant mice in terms of the body and TA muscle weights at 2 weeks after injection (Fig. 3G). Immunofluorescence staining of perilipin in conjunction with laminin (Fig. 3H) revealed no significant difference in the minimal Ferret diameter of myofibers or the area occupied by adipocytes between the control and mutant TA muscles (Fig. 3I). These findings suggest that the absence of AR in mesenchymal progenitors does not significantly affect the adipogenic properties of TA muscles.

AR deficiency in mesenchymal progenitors in mature adult and aged mice modestly affected limb skeletal muscles

To examine the long-term impact of AR ablation on mesenchymal progenitors, we analyzed mature adult (6 months old) and aged (28 months old) mice and compared the Cre control group and mutant group (Fig. 4A). In the mature adult mutant mice, we observed decreases in body weight and TA and gastrocnemius muscle weights (Fig. 4B), while there were no significant changes in the weights of the epidermal and subcutaneous white adipose tissues (Fig. 4B), which are affected by systemic AR ablation (34). However, grip strength (Fig. 4C) and the fiber-type parameters, including the minimal Ferret diameter and frequency of each fiber-type (Fig. 4D and 4E), were comparable between the control and mutant mice.

Additionally, the weights of the entire body, hindlimb muscles, and white adipose tissues were compared between aged control and mutant mice. At 28 months of age, the mutant mice did not exhibit any significant differences from the control mice (Fig. 4F). Moreover, the mutant mice exhibited similar grip strength to that of the control mice (Fig. 4G). Therefore, our findings demonstrate that AR deficiency in mesenchymal progenitors affects skeletal muscle mass in mature adult mice only, not young or aged mice, primarily in the limbs.

Mesenchymal progenitor-specific AR ablation induced atrophy of LA/BC muscles

The perineal LA/BC skeletal muscle complex exhibits increased responsiveness to androgens compared with other striated muscles (35). Because this perineal muscle complex also has higher AR expression (14), we examined the impact of AR ablation on mesenchymal progenitors of LA/BC skeletal muscles. We confirmed efficient ablation of AR in PDGFRα+ cells in LA muscles as well as limb muscles (Fig. 5A, B). At 14 weeks, 6 months, and 28 months of age, the

LA/BC mass was consistently lower in the mutant mice than control mice (Fig. 5C). Because AR ablation in myofibers (*HSA-Cre*$^{Tg/+}$*;AR*$^{L2/Y}$ mice) also leads to reduced LA/BC mass (36), we generated *HSA-Cre*$^{Tg/+}$*;PDGFRα-CreER;AR*$^{L2/Y}$ mice to examine whether the weight reduction depended on AR in myofibers. Interestingly, the LA/BC weight was lower in *HSA-Cre*$^{Tg/+}$*;AR*$^{L2/Y}$ mice than in *PDGFRα-CreER;AR*$^{L2/Y}$ mice (Fig. 5D). Moreover, *HSA-Cre*$^{Tg/+}$*;PDGFRα-CreER;AR*$^{L2/Y}$ mice had the lowest LA/BC mass compared with *HSA-Cre*$^{Tg/+}$*;AR*$^{L2/Y}$ and *PDGFRα-CreER;AR*$^{L2/Y}$ mice (Fig. 5D). These findings suggest that AR expression in both myofibers and mesenchymal progenitors independently regulates the mass of perineal muscles. We also found that AR depletion in mesenchymal progenitors in LA muscles led to a decrease in the number of PDGFRα+ cells (Fig. 5E). Examination of the cross-sectional area of LA muscles by laminin staining (Fig. 5F) revealed a lower myofiber size in the mutant mice than control mice (Fig. 5G). In summary, AR expression in mesenchymal progenitors independently regulates the mass of perineal muscles, separate from its influence on myofibers.

AR in mesenchymal progenitors regulated Igf1 expression

To determine the effects of AR on gene expression, we performed RNA-seq in PDGFRα+ cells from the LA/BC muscles of both control and mutant mice (Fig. 6A). Using a previously established gating strategy for isolating mesenchymal progenitors (CD45− CD31− Vcam1− PDGFRα+) (12) (Fig. 6B), we isolated 300 PDGFRα+ cells for RNA-seq. We detected more than 100,000 genes in these cells, indicating sufficient read depth for further analysis (Fig. 6C). The PCA plot showed separation between the control and mutant samples (Fig. 6E). We identified 80 upregulated and 76 downregulated genes, including AR, in PDGFRα+ cells from the mutant mice (Fig. 6E). The upregulated genes were enriched in the Gene Ontology terms

including regulation of cell death and cell motility (Fig. 6F). On the other hand, the downregulated genes were enriched in the Gene Ontology terms related to extracellular matrix organization and regulation of proteolysis (Fig. 6G). Among the genes differentially expressed after AR depletion, we focused on *Igf1*, which is critical for maintaining muscle mass (37). *Igf1* was downregulated in the mutant PDGFRα+ cells (Fig. 6H). To further investigate the effects of androgen and AR on *Igf1* expression, we isolated PDGFRα+ cells from C57BL/6J mice treated with DHT (Fig. 6I). We found upregulation of *Igf1* in PDGFRα+ cells after DHT administration (Fig. 6J). We also found an androgen response element in the promoter region of *Igf1* (Fig. 6K). Taken together, AR in mesenchymal progenitors regulates *Igf1* expression.

Discussion

In the present study, we demonstrated that mice with specific AR ablation in mesenchymal progenitors showed lower skeletal muscle mass in the limbs only at the mature adult stage, but not at a younger stage (14 weeks old). Taken together with previous reports demonstrating that mice with AR ablation specifically in fast-twitch fibers lack muscle mass reduction at 13 weeks old but exhibit this reduction at 12–13 months old (32), there may be a potential age-dependent role of AR or an effect that requires time to develop. Additionally, we demonstrated that the number of Pax7+ muscle stem cells was similar between adult control and mutant mice. This is in contrast to the observed reduction in myoblast proliferation following deletion of AR in the mesenchyme of BC muscles during development (16), providing evidence that AR in mesenchymal progenitors plays distinct roles during development, adulthood, and aging in mice. We also showed that specific ablation of AR in mesenchymal progenitors does not affect the fiber types of slow-twitch muscles. Depletion of mesenchymal progenitors results in a slight increase in the proportion of slow fibers (type I) predominantly in fast-twitch TA muscles (12), suggesting that factors other than AR in mesenchymal progenitors influence muscle fiber types.

PDGFRα+ cells are the origin of ectopic adipocytes in skeletal muscles (9,38). However, the specific molecular mechanisms underlying fatty infiltration of muscles remain largely unexplored (39). In general, androgen and AR signaling seem to have inhibitory effects on adipogenesis (40). Serum androgens are linked to reduced levels of fatty infiltration of skeletal muscles (41). In contrast, deprivation of androgens leads to an increase in fatty infiltration of skeletal muscle in men (42). Moreover, transgenic mice expressing AR induced by collagen type I alpha 1, which is also expressed in mesenchymal progenitors (43), have reduced body weight and fat mass (44). Additionally, HFD-induced fat mass deposition in skeletal muscles was

increased by a low androgen level caused by orchiedectomy (45). However, our results indicate that AR deficiency in mesenchymal progenitors does not affect adipogenesis in skeletal muscle even after HFD feeding or glycerol injection. An indirect androgen pathway may also regulate adipogenesis of mesenchymal progenitors in skeletal muscles. Indeed, recent research indicates that androgens can modulate macrophage polarization, subsequently affecting adipocyte differentiation (46). Further studies are needed to gain a comprehensive understanding of the mechanisms by which androgens and AR signaling influence fatty infiltration of muscle.

We observed a modest reduction in the muscle weight of the mutant mice at the mature adult age (24 weeks old), but this effect was not observed in aged mice (28 months old). Because selective ablation of AR in myofibers does not lead to reduced muscle mass even in 40-week-old mice (36), the role of AR in mesenchymal progenitors is more important than its role in myofibers in the context of muscle maintenance, at least at the mature adult age. A decrease in testosterone concentration, even in 1-year-old mice compared with young 12-week-old mice (47), may contribute to muscle mass loss, potentially masking any subtle differences between the aged control and mutant mice. Due to the reduction in muscle mass observed in 2-year-old mice with AR depletion specifically in fast-twitch fibers (32), AR expression in muscle fibers may play a crucial role in regulating muscle metabolism and quality, which help maintain muscle mass in aged mice.

The perineal skeletal muscles LA and BC are highly androgen sensitive. Muscle fiber-specific AR knockout results in a more pronounced mass reduction in LA/BC muscles compared with limb muscles (35,36), which is consistent with our present study demonstrating a consistent reduction in LA/BC muscles in mice with AR ablation in mesenchymal progenitors. We also demonstrated that AR deficiency in mesenchymal progenitors resulted in reduced LA/BC weight,

although the extent of the reduction was milder compared with mice with AR ablation in muscle fibers. Furthermore, the double Cre mice (*HSA-Cre*$^{Tg/+}$*;PDGFRα-CreER;AR*$^{L2/Y}$), with ablation of AR in both myofibers and mesenchymal progenitors, exhibited a greater reduction in LA/BC mass compared with single Cre mice (*HSA-Cre*$^{Tg/+}$*;AR*$^{L2/Y}$ or *PDGFRα-CreER;AR*$^{L2/Y}$). Taken together, AR expression in mesenchymal progenitors independently regulates the mass of perineal muscles, separate from the influence of AR in myofibers. The distinct reactions observed in perineal and limb muscles could be attributed to a greater abundance of myonuclei expressing AR in perineal muscles compared with limb muscles (14). Nevertheless, our findings revealed that the majority of PDGFRα+ cells exhibited AR expression in both limb and perineal muscles, suggesting an additional mechanism by which AR in mesenchymal progenitors regulates muscle mass and other mesenchymal progenitor functions.

The signaling pathway involving IGF1 plays a crucial role in both the developmental growth and steady-state maintenance of skeletal muscle mass (48,49). IGF1 is produced primarily in the liver (50), but local production, including in skeletal muscles, is induced by androgen treatment. The administration of testosterone to older men led to an increase in IGF1 protein expression in the limb (vastus lateralis) muscles (51). *Igf1* expression is decreased in the LA/BC muscles of mice with skeletal muscle-specific AR ablation (36). Dubois et al. suggested indirect androgen regulation of IGF1 via non myocytic AR because Myod-Cre-driven AR-deficient mice show no reduction in the *Igf1* transcript level, and Igf1 expression is decreased after castration in skeletal muscles (28). We demonstrated that AR in mesenchymal progenitors in skeletal muscles regulates *Igf1* expression, governing muscle mass. Moreover, activation of Akt signaling via the expression of Bmp3b in mesenchymal progenitors (12) suggests a

connection with Igf1, highlighting the complex interplay of signaling pathways in the maintenance of skeletal muscle mass.

In summary, our results show that AR in mesenchymal progenitors regulates skeletal muscle mass via Igf1 expression. Additional investigations into AR function in mesenchymal progenitors, including ChIP-seq analysis targeting AR, are needed to confirm the role of AR in regulating the differentially expressed genes in AR-ablated mesenchymal progenitors. Combining treatment with androgens and Igf1 could be useful to treat muscle atrophy such as sarcopenia.

Acknowledgments

We thank A. Nishio and Y. Sato for their technical support, Y. Tanaka for the flow cytometry support, and other members of the Division of Medical Research Support, the Advanced Research Support Center, Ehime University. This study was partly performed in the Cooperative Research Project Program in the Medical Institute of Bioregulation (MIB), Kyushu University. We also thank the Medical Research Center for High Depth Omics, MIB, Kyushu University for the sequencing, and RIST at Kyushu University for the high-performance computing.

Data Availability

RNA-seq data have been deposited in the Gene Expression Omnibus as accession number GSE247378 and are publicly available as of the date of publication.

References

1. **Papanicolaou GN, Falk EA.** General Muscular Hypertrophy Induced by Androgenic Hormone. *Science* 1938;87(2254):238–239.

2. **Bhasin S, Storer TW, Berman N, Callegari C, Clevenger B, Phillips J, Bunnell TJ, Tricker R, Shirazi A, Casaburi R.** The Effects of Supraphysiologic Doses of Testosterone on Muscle Size and Strength in Normal Men. *N. Engl. J. Med.* 1996;335(1):1–7.

3. **Lubahn DB, Joseph DR, Sullivan PM, Willard HF, French FS, Wilson EM.** Cloning of Human Androgen Receptor Complementary DNA and Localization to the X Chromosome. *Science* 1988;240(4850):327–330.

4. **Lincoff AM, Bhasin S, Flevaris P, Mitchell LM, Basaria S, Boden WE, Cunningham GR, Granger CB, Khera M, Thompson IM, Wang Q, Wolski K, Davey D, Kalahasti V, Khan N, Miller MG, Snabes MC, Chan A, Dubcenco E, Li X, Yi T, Huang B, Pencina KM, Travison TG, Nissen SE, Investigators TS.** Cardiovascular Safety of Testosterone-Replacement Therapy. *N. Engl. J. Med.* 2023;389(2):107–117.

5. **MacLean HE, Chiu WSM, Notini AJ, Axell A-M, Davey RA, McManus JF, Ma C, Plant DR, Lynch GS, Zajac JD.** Impaired skeletal muscle development and function in male, but not female, genomic androgen receptor knockout mice. *FASEB J.* 2008;22(8):2676–2689.

6. **Sakakibara I, Yanagihara Y, Himori K, Yamada T, Sakai H, Sawada Y, Takahashi H, Saeki N, Hirakawa H, Yokoyama A, Fukada S, Sawasaki T, Imai Y.** Myofiber androgen receptor increases muscle strength mediated by a skeletal muscle splicing variant of Mylk4. *iScience* 2021;24(4):102303.

7. **Sakai H, Sato T, Kanagawa M, Fukada S, Imai Y.** Androgen receptor in satellite cells is not essential for muscle regenerations. *Exp. Results* 2020;1. doi:10.1017/exp.2020.14.

8. **Dubois V, Laurent MR, Sinnesael M, Cielen N, Helsen C, Clinckemalie L, Spans L, Gayan□Ramirez G, Deldicque L, Hespel P, Carmeliet G, Vanderschueren D, Claessens F.** A satellite cell□specific knockout of the androgen receptor reveals myostatin as a direct androgen target in skeletal muscle. *FASEB J.* 2014;28(7):2979–2994.

9. **Uezumi A, Fukada S, Yamamoto N, Takeda S, Tsuchida K.** Mesenchymal progenitors distinct from satellite cells contribute to ectopic fat cell formation in skeletal muscle. *Nat Cell Biol* 2010;12(2):143–152.

10. **Joe AWB, Yi L, Natarajan A, Grand FL, So L, Wang J, Rudnicki MA, Rossi FMV.** Muscle injury activates resident fibro/adipogenic progenitors that facilitate myogenesis. *Nat Cell Biol* 2010;12(2):153–163.

11. **Wosczyna MN, Konishi CT, Carbajal EEP, Wang TT, Walsh RA, Gan Q, Wagner MW, Rando TA.** Mesenchymal Stromal Cells Are Required for Regeneration and Homeostatic Maintenance of Skeletal Muscle. *Cell Reports* 2019;27(7):2029-2035.e5.

12. **Uezumi A, Ikemoto-Uezumi M, Zhou H, Kurosawa T, Yoshimoto Y, Nakatani M, Hitachi K, Yamaguchi H, Wakatsuki S, Araki T, Morita M, Yamada H, Toyoda M, Kanazawa N, Nakazawa T, Hino J, Fukada S, Tsuchida K.** Mesenchymal Bmp3b expression maintains skeletal muscle integrity and decreases in age-related sarcopenia. *J Clin Invest* 2020;131(1). doi:10.1172/jci139617.

13. **Uezumi A, Ito T, Morikawa D, Shimizu N, Yoneda T, Segawa M, Yamaguchi M, Ogawa R, Matev MM, Miyagoe-Suzuki Y, Takeda S, Tsujikawa K, Tsuchida K, Yamamoto H, Fukada S.** Fibrosis and adipogenesis originate from a common mesenchymal progenitor in skeletal muscle. *J Cell Sci* 2011;124(21):3654–3664.

14. **Johansen JA, Breedlove SM, Jordan CL.** Androgen Receptor Expression in the Levator Ani Muscle of Male Mice. *J Neuroendocrinol* 2007;19(10):823–826.

15. **Sinha-Hikim I, Taylor WE, Gonzalez-Cadavid NF, Zheng W, Bhasin S.** Androgen Receptor in Human Skeletal Muscle and Cultured Muscle Satellite Cells: Up-Regulation by Androgen Treatment. *J Clin Endocrinol Metabolism* 2004;89(10):5245–5255.

16. **Ipulan LA, Suzuki K, Sakamoto Y, Murashima A, Imai Y, Omori A, Nakagata N, Nishinakamura R, Valasek P, Yamada G.** Nonmyocytic Androgen Receptor Regulates the Sexually Dimorphic Development of the Embryonic Bulbocavernosus Muscle. *Endocrinology* 2014;155(7):2467–2479.

17. **Kang SH, Fukaya M, Yang JK, Rothstein JD, Bergles DE.** NG2+ CNS Glial Progenitors Remain Committed to the Oligodendrocyte Lineage in Postnatal Life and following Neurodegeneration. *Neuron* 2010;68(4):668–681.

18. **Miniou P, Tiziano D, Frugier T, Roblot N, Meur ML, Melki J.** Gene targeting restricted to mouse striated muscle lineage. *Nucleic Acids Res.* 1999;27(19):e27–e30.

19. **Matsumoto T, Takeyama K, Sato T, Kato S.** Androgen receptor functions from reverse genetic models. *J. Steroid Biochem. Mol. Biol.* 2003;85(2–5):95–99.

20. **Arsic N, Zacchigna S, Zentilin L, Ramirez-Correa G, Pattarini L, Salvi A, Sinagra G, Giacca M.** Vascular endothelial growth factor stimulates skeletal muscle regeneration in Vivo. *Mol Ther* 2004;10(5):844–854.

21. **Liu L, Cheung TH, Charville GW, Rando TA.** Isolation of skeletal muscle stem cells by fluorescence-activated cell sorting. *Nat Protoc* 2015;10(10):1612–1624.

22. **Hashimshony T, Senderovich N, Avital G, Klochendler A, Leeuw Y de, Anavy L, Gennert D, Li S, Livak KJ, Rozenblatt-Rosen O, Dor Y, Regev A, Yanai I.** CEL-Seq2: sensitive highly-multiplexed single-cell RNA-Seq. *Genome Biol* 2016;17(1):77.

23. **Smith T, Heger A, Sudbery I.** UMI-tools: modeling sequencing errors in Unique Molecular Identifiers to improve quantification accuracy. *Genome Res.* 2017;27(3):491–499.

24. **Kim D, Paggi JM, Park C, Bennett C, Salzberg SL.** Graph-based genome alignment and genotyping with HISAT2 and HISAT-genotype. *Nat Biotechnol* 2019;37(8):907–915.

25. **Liao Y, Smyth GK, Shi W.** featureCounts: an efficient general purpose program for assigning sequence reads to genomic features. *Bioinformatics* 2014;30(7):923–930.

26. **Love MI, Huber W, Anders S.** Moderated estimation of fold change and dispersion for RNA-seq data with DESeq2. *Genome Biol* 2014;15(12):550.

27. **Zhou Y, Zhou B, Pache L, Chang M, Khodabakhshi AH, Tanaseichuk O, Benner C, Chanda SK.** Metascape provides a biologist-oriented resource for the analysis of systems-level datasets. *Nat Commun* 2019;10(1):1523.

28. **Dubois V, Simitsidellis I, Laurent MR, Jardi F, Saunders PTK, Vanderschueren D, Claessens F.** Enobosarm (GTx-024) Modulates Adult Skeletal Muscle Mass Independently of the Androgen Receptor in the Satellite Cell Lineage. *Endocrinology* 2015;156(12):4522–4533.

29. **Kanou M, Nakamura K, Horie K, Sakai H, Yanagihara Y, Sakakibara I, Yamana K, Imai Y.** Polyamine pathway is associated with muscle anabolic effects by androgen receptor ligand. *Jcsm Rapid Commun* 2021;4(1):57–74.

30. **Kaneshige A, Kaji T, Zhang L, Saito H, Nakamura A, Kurosawa T, Ikemoto-Uezumi M, Tsujikawa K, Seno S, Hori M, Saito Y, Matozaki T, Maehara K, Ohkawa Y, Potente M, Watanabe S, Braun T, Uezumi A, Fukada S.** Relayed signaling between mesenchymal progenitors and muscle stem cells ensures adaptive stem cell response to increased mechanical load. *Cell Stem Cell* 2022;29(2):265-280.e6.

31. **Seale P, Sabourin LA, Girgis-Gabardo A, Mansouri A, Gruss P, Rudnicki MA.** Pax7 Is Required for the Specification of Myogenic Satellite Cells. *Cell* 2000;102(6):777–786.

32. **Hosoi T, Yakabe M, Sasakawa H, Sasako T, Ueki K, Kato S, Tokuoka SM, Oda Y, Abe M, Matsumoto T, Akishita M, Ogawa S.** Sarcopenia phenotype and impaired muscle function in male mice with fast-twitch muscle-specific knockout of the androgen receptor. *Proc. Natl. Acad. Sci.* 2023;120(4):e2218032120.

33. **Greenberg AS, Egan JJ, Wek SA, Garty NB, Blanchette-Mackie EJ, Londos C.** Perilipin, a major hormonally regulated adipocyte-specific phosphoprotein associated with the periphery of lipid storage droplets. *J. Biol. Chem.* 1991;266(17):11341–11346.

34. **Fan W, Yanase T, Nomura M, Okabe T, Goto K, Sato T, Kawano H, Kato S, Nawata H.** Androgen Receptor Null Male Mice Develop Late-Onset Obesity Caused by Decreased Energy Expenditure and Lipolytic Activity but Show Normal Insulin Sensitivity With High Adiponectin Secretion. *Diabetes* 2005;54(4):1000–1008.

35. **Ophoff J, Proeyen KV, Callewaert F, Gendt KD, Bock KD, Bosch AV, Verhoeven G, Hespel P, Vanderschueren D.** Androgen Signaling in Myocytes Contributes to the Maintenance of Muscle Mass and Fiber Type Regulation But Not to Muscle Strength or Fatigue. *Endocrinology* 2009;150(8):3558–3566.

36. **Chambon C, Duteil D, Vignaud A, Ferry A, Messaddeq N, Malivindi R, Kato S, Chambon P, Metzger D.** Myocytic androgen receptor controls the strength but not the mass of limb muscles. *Proc. Natl. Acad. Sci.* 2010;107(32):14327–14332.

37. **Rommel C, Bodine SC, Clarke BA, Rossman R, Nunez L, Stitt TN, Yancopoulos GD, Glass DJ.** Mediation of IGF-1-induced skeletal myotube hypertrophy by PI(3)K/Akt/mTOR and PI(3)K/Akt/GSK3 pathways. *Nat Cell Biol* 2001;3(11):1009–1013.

38. **Joe AWB, Yi L, Natarajan A, Grand FL, So L, Wang J, Rudnicki MA, Rossi FMV.** Muscle injury activates resident fibro/adipogenic progenitors that facilitate myogenesis. *Nat Cell Biol* 2010;12(2):153–163.

39. **Hamrick MW, McGee-Lawrence ME, Frechette DM.** Fatty Infiltration of Skeletal Muscle: Mechanisms and Comparisons with Bone Marrow Adiposity. *Front. Endocrinol.* 2016;7:69.

40. **Rizk J, Sahu R, Duteil D.** An overview on androgen-mediated actions in skeletal muscle and adipose tissue. *Steroids* 2023;199:109306.

41. **Miljkovic I, Cauley JA, Dressen AS, Gordon CL, Goodpaster BH, Kuller LH, Bunker CH, Patrick AL, Wheeler VW, Orwoll ES, Zmuda JM.** Bioactive androgens and glucuronidated androgen metabolites are associated with subcutaneous and ectopic skeletal muscle adiposity among older black men. *Metabolism* 2011;60(8):1178–1185.

42. **Chang D, Joseph DJ, Ebert MA, Galvão DA, Taaffe DR, Denham JW, Newton RU, Spry NA.** Androgen deprivation muscle attenuation. *J. Méd. Imaging Radiat. Oncol.* 2014;58(2):223–228.

43. **Chapman MA, Mukund K, Subramaniam S, Brenner D, Lieber RL.** Three distinct cell populations express extracellular matrix proteins and increase in number during skeletal muscle fibrosis. *Am J Physiol-cell Ph* 2017;312(2):C131–C143.

44. **Semirale AA, Zhang X, Wiren KM.** Body composition changes and inhibition of fat development in vivo implicates androgen in regulation of stem cell lineage allocation. *J. Cell. Biochem.* 2011;112(7):1773–1786.

45. **Dubois V, Laurent MR, Jardi F, Antonio L, Lemaire K, Goyvaerts L, Deldicque L, Carmeliet G, Decallonne B, Vanderschueren D, Claessens F.** Androgen Deficiency Exacerbates High-Fat Diet-Induced Metabolic Alterations in Male Mice. *Endocrinology* 2016;157(2):648–665.

46. **Ren X, Fu X, Zhang X, Chen S, Huang S, Yao L, Liu G.** Testosterone regulates 3T3-L1 pre-adipocyte differentiation and epididymal fat accumulation in mice through modulating macrophage polarization. *Biochem. Pharmacol.* 2017;140:73–88.

47. **Nilsson ME, Vandenput L, Tivesten sa, Norlén A-K, Lagerquist MK, Windahl SH, Börjesson AE, Farman HH, Poutanen M, Benrick A, Maliqueo M, Stener-Victorin E, Ryberg H, Ohlsson C.** Measurement of a Comprehensive Sex Steroid Profile in Rodent Serum by High-Sensitive Gas Chromatography-Tandem Mass Spectrometry. *Endocrinology* 2015;156(7):2492–2502.

48. **O'Neill BT, Lee KY, Klaus K, Softic S, Krumpoch MT, Fentz J, Stanford KI, Robinson MM, Cai W, Kleinridders A, Pereira RO, Hirshman MF, Abel ED, Accili D, Goodyear LJ, Nair KS, Kahn CR.** Insulin and IGF-1 receptors regulate FoxO-mediated signaling in muscle proteostasis. *J Clin Invest* 2016;126(9):3433–3446.

49. **Ascenzi F, Barberi L, Dobrowolny G, Bacurau AVN, Nicoletti C, Rizzuto E, Rosenthal N, Scicchitano BM, Musarò A.** Effects of IGF 1 isoforms on muscle growth and sarcopenia. *Aging Cell* 2019;18(3):e12954.

50. **Kineman RD, Rio-Moreno M del, Sarmento-Cabral A.** 40 YEARS of IGF1: Understanding the tissue-specific roles of IGF1/IGF1R in regulating metabolism using the Cre/loxP system. *J. Mol. Endocrinol.* 2018;61(1):T187–T198.

51. **Ferrando AA, Sheffield-Moore M, Yeckel CW, Gilkison C, Jiang J, Achacosa A, Lieberman SA, Tipton K, Wolfe RR, Urban RJ.** Testosterone administration to older men improves muscle function: molecular and physiological mechanisms. *Am. J. Physiol.-Endocrinol. Metab.* 2002;282(3):E601–E607.

52. **Ghaibour K, Schuh M, Souali Crespo S, Chambon C, Charlot A, Rizk J, Rovito D, Rerra A, Cai Q, Messaddeq N, Zoll J, Duteil D, Metzger D.** Androgen receptor coordinates muscle metabolic and contractile functions. *J. Cachexia, Sarcopenia Muscle* 2023;14(4):1707–1720.

Legends for Figures

Figure 1. AR ablation in mesenchymal progenitors from *PDGFRα-CreER;AR*$^{L2/Y}$ mice. (A) Immunofluorescence staining of AR (left) and PDGFRα (middle) and of both together with laminin and DAPI staining (right) in male TA muscles. Arrows: AR+ and PDGFRα+ cells; arrowheads: AR+ nuclei surrounded by laminin. Scale bar, 50 µm. (B) Experimental design for TMX treatment followed by sample harvest. (C) Quantification of AR+ cells among PDGFRα+ cells in the BB (left) and TA (right) muscles of control and mutant mice (n = 3). The two-sample test for equality of proportions was performed using the test of equal or given proportions: ***p < 0.001, ****p < 0.0001. (D) Quantification of PDGFRα+ cells in the BB (left) and TA (right) muscles of control and mutant mice.

Figure 2. Limited impact of AR deficiency in mesenchymal progenitors on intact limb skeletal muscles. (A) Experimental design for TMX treatment followed by sample harvest. (B and C) Quantification of body weight, muscle mass (B) and grip strength (C) at 2 weeks after TMX treatment (n = 8 control; n = 9 mutant mice). (D and E) Violin plots of the minimal Ferret diameters of each individual (top) with their mean (bottom left) and quantification of the number of muscle fibers (bottom right) in the BB (D) and TA (E) muscles of control and mutant mice (n = 6). (F) Quantification of the number of Pax7+ cells in BB (top) and TA (bottom) muscles of control and mutant mice (n = 6). (G) Immunofluorescence staining of Myh7, Myh2, and laminin in the soleus muscles of control (left) and mutant mice (right). Scale bar, 100 µm. (H) Average minimal Ferret diameter (left) and frequency (right) of each fiber type in control and mutant mice (n = 3).

Figure 3. Limited impact of AR deficiency in mesenchymal progenitors on adipogenesis in muscles. (A) Experimental design for TMX treatment followed by HFD feeding. (B and C) Quantification of body weight (BW), muscle mass, eWAT mass, sWAT mass (B), and grip strength (C) at 8 weeks after HFD feeding (n = 7 control; n = 9 mutant mice). (D) Immunofluorescence staining of perilipin and laminin in TA muscles of control (left) and mutant mice (right) after HFD feeding. Scale bar, 100 µm. (E) Average minimal Ferret diameter (left) and perilipin+ area in TA muscles (n = 5 control; n = 7 mutant mice). (F) Experimental design for TMX treatment followed by glycerol injection. (G) Quantification of BW and TA muscle mass at 2 weeks after glycerol injection (n = 6). (H) Perilipin and laminin immunofluorescence staining in the TA muscles of control (left) and mutant mice (right) after glycerol injection. Scale bar, 500 µm. (I) Average minimal Ferret diameter (left) and perilipin+ area of TA muscles after glycerol injection (n = 6).

Figure 4. Modest impact of AR deficiency in mesenchymal progenitors on limb muscles in mature adult and aged mice. (A) Experimental design for TMX treatment followed by sample harvest in mature adult (6 months old) and aged (28 months old) mice. (B and C) Quantification of body weight (BW), muscle mass, eWAT mass, sWAT mass (B), and grip strength (C) in 6-month-old mice (n = 7 control; n = 10 mutant mice). Unpaired t-test with Welch's correction: *p < 0.05, **p < 0.01. (D) Immunofluorescence staining of Myh2, Myh4, and laminin in TA muscles of control (left) and mutant (right) mice. Scale bar, 500 µm. (E) Average minimal Ferret diameter (left) and frequency (right) of each fiber type in control and mutant mice (n = 6). (F and G) Quantification of BW, muscle mass, eWAT mass, sWAT mass (F), and grip strength (G) in 28-month-old mice (n = 6 control; n = 7 mutant mice).

Figure 5. Atrophy of LA/BC muscles in mesenchymal progenitor-specific AR-deficient mice. (A) Immunofluorescence staining of AR, PDGFRα, and laminin with DAPI in LA muscles of control (left) and mutant (right) mice. Scale bar, 10 µm. (B) Quantification of AR+ cells among PDGFRα+ cells in LA muscles of control and mutant mice (n = 3). The two-sample test for equality of proportions was performed using the test of equal or given proportions: ***$p < 0.001$. (C) Mass of LA/BC muscles in 14-week-, 6-month-, and 28-month-old mice (n = 5–12). (D) Mass of LA/BC muscles in single (*HSA-Cre* or *PDGFRα-CreER*) and double Cre mice. (E) Quantification of PDGFRα+ cells in LA muscles of control and mutant mice (n = 3). Unpaired t-test with Welch's correction: *$p < 0.05$. (F) Immunofluorescence staining of laminin in LA muscles of control (left) and mutant mice (right). Scale bar, 500 µm. (G) Average cross-sectional area (CSA) of myofibers in control and mutant mice (n = 3). Unpaired t-test with Welch's correction: *$p < 0.05$.

Figure 6. Regulation of *Igf1* in mesenchymal progenitors by AR. (A) Experimental design for TMX treatment followed by fluorescence-activated cell sorting (FACS) and RNA-seq. (B) FACS gating for isolating mesenchymal progenitors (PDGFRα+ Vcam1− CD45− CD31−) for RNA-seq. (C) Gene counts detected in each RNA-seq sample (n = 5). (D) PCA plot of the RNA-seq samples. (E) Volcano plot showing the $\log_2$ fold change (LFC, x-axis) and $-\log_{10}$ q-value (y-axis) of each gene in the differential expression analysis; red dots: DESeq2, LFC > 0, $q < 0.1$; blue dots: DESeq2, LFC < 0, $q < 0.1$. Positive and negative FC values indicate upregulated and downregulated genes, respectively, in PDGFRα+ cells from mutant mice. (F and G) Top Gene Ontology biological process terms associated with the upregulated (F) and downregulated (G)

genes in PDGFRα+ cells from mutant mice. (H) Normalized gene counts for *Igf1* obtained by RNA-seq. (I) Experimental design for qPCR after treatment with DHT. (J) qPCR analysis of Igf1 in PDGFRα+ cells after DHT treatment (n = 3 mice/condition). Unpaired t-test with Welch's correction: *$p < 0.05$. (K) Androgen response elements (ARE) located near the *Igf1* loci.

Table 1. Oligonucleotides used in this study.

Oligo name	Sequence	Additional information
Igf1_F	TGGATGCTCTTCAGTTCGTG	qPCR
Igf1_R	CACTCATCCACAATGCCTGT	qPCR
Rpl13a_F	GTGGTCCCTGCTGCTCTCAAG	qPCR
Rpl13a_R	CGATAGTGCATCTTGGCCTTTT	qPCR

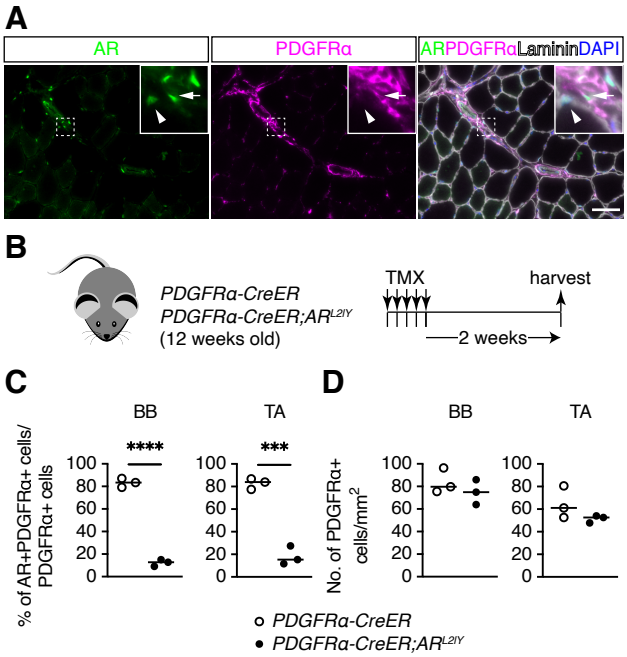

Figure 1 Sakai et al.

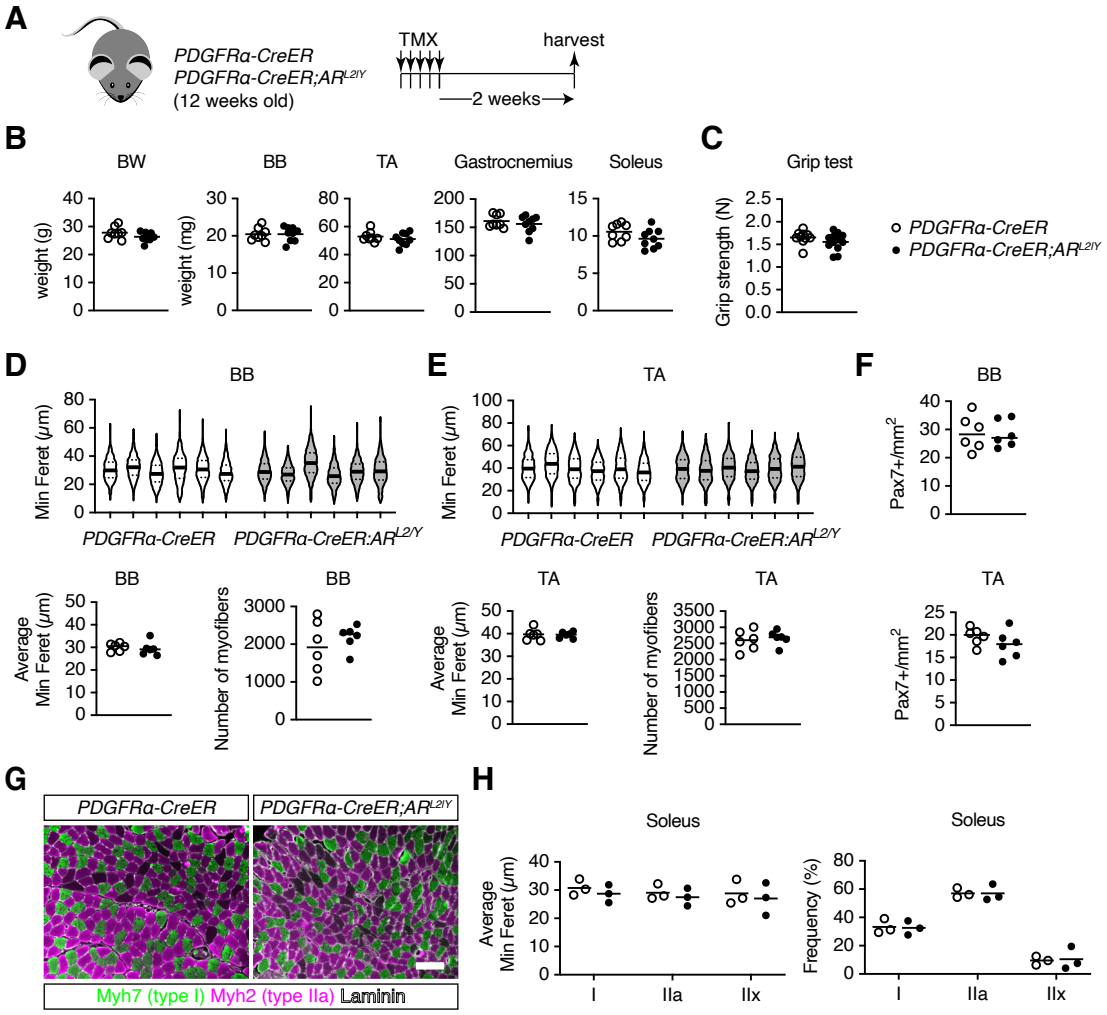

Figure 2 Sakai et al.

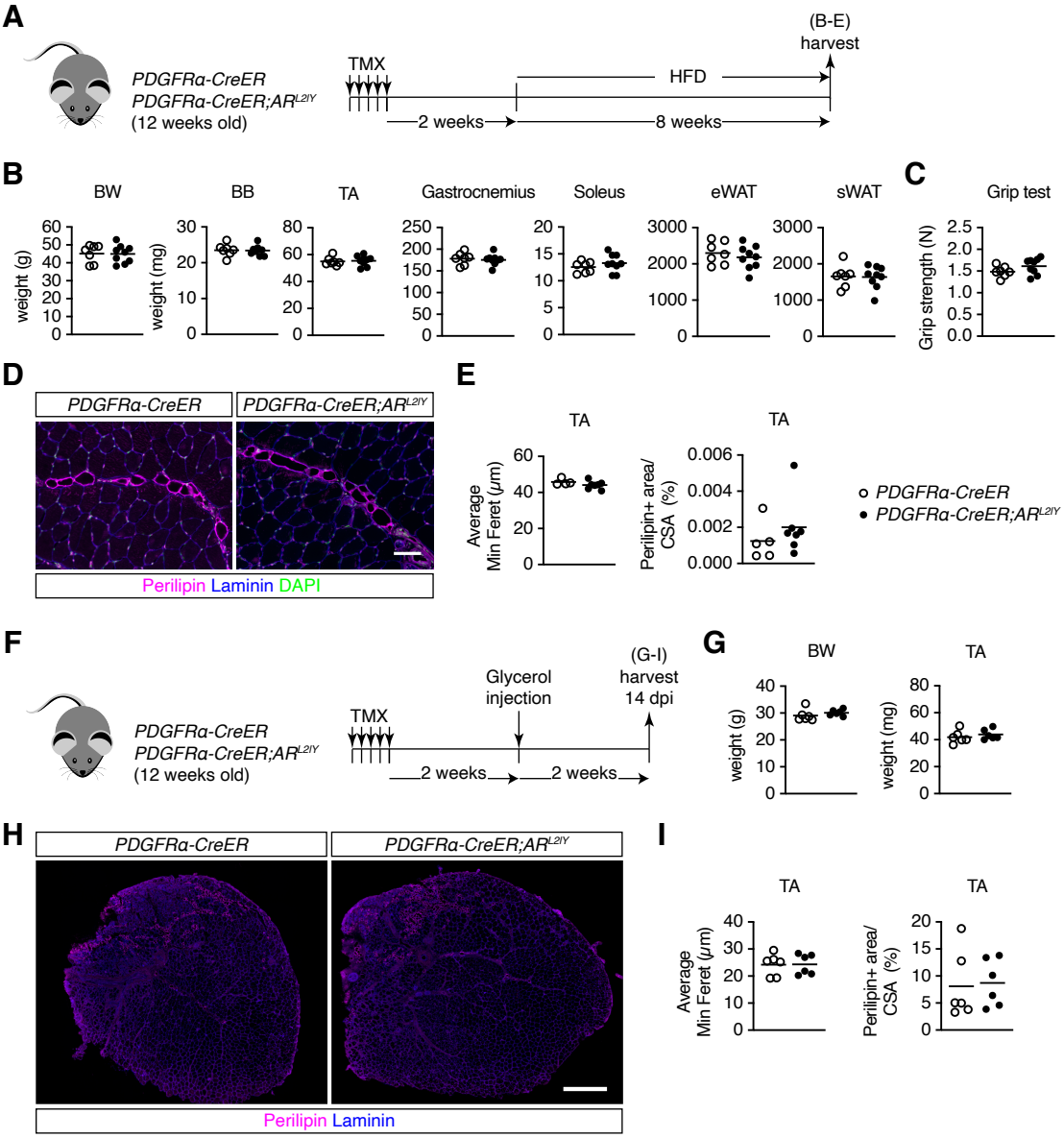

Figure 3 Sakai et al.

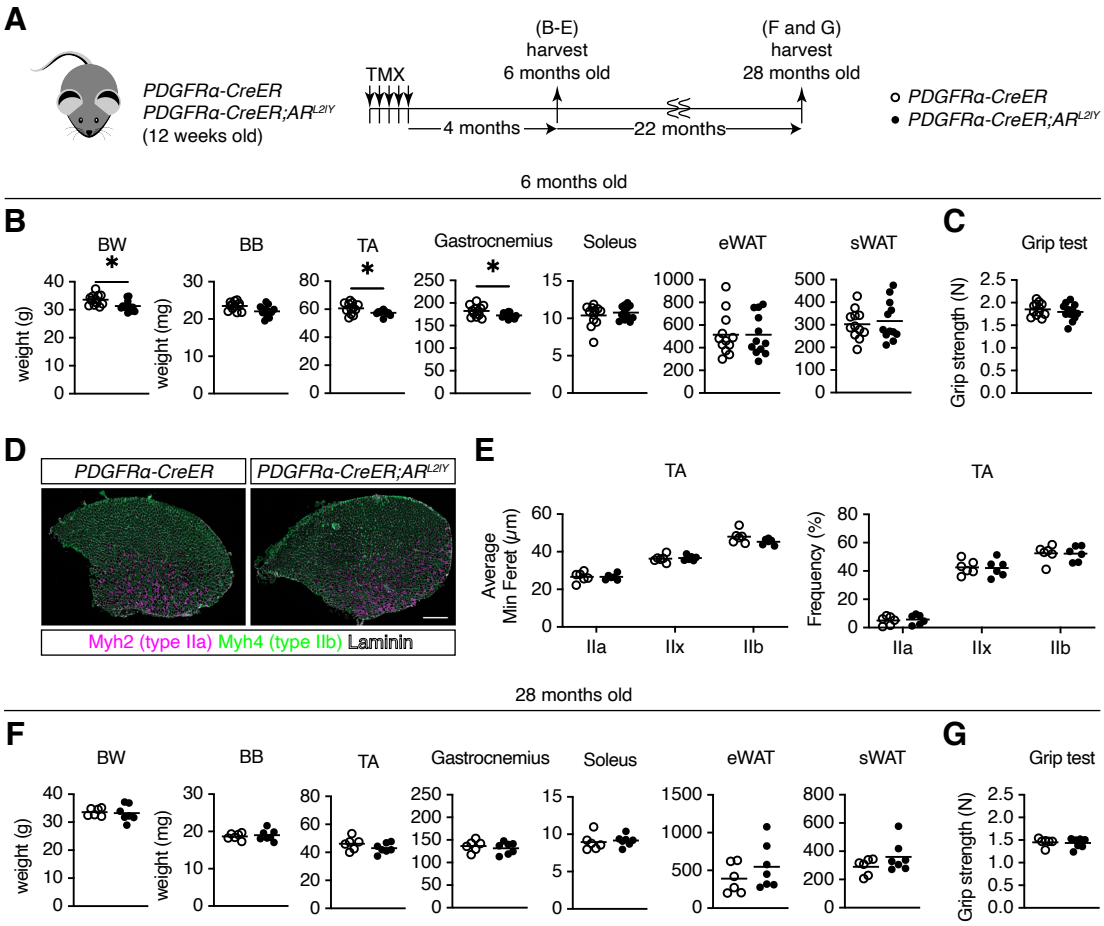

Figure 4 Sakai et al.

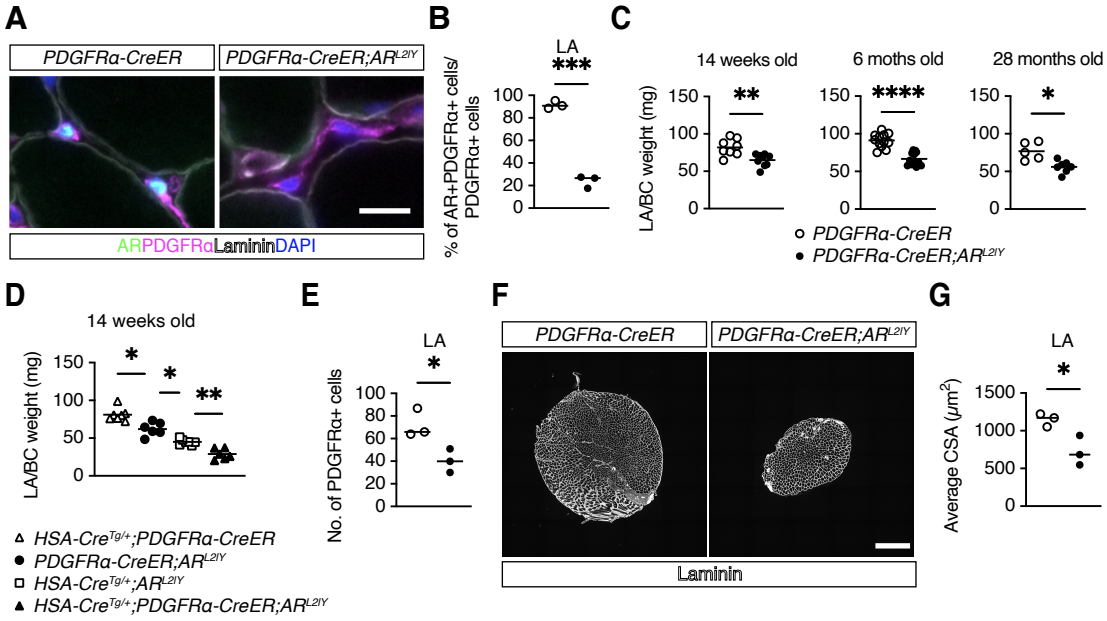

Figure 5 Sakai et al.

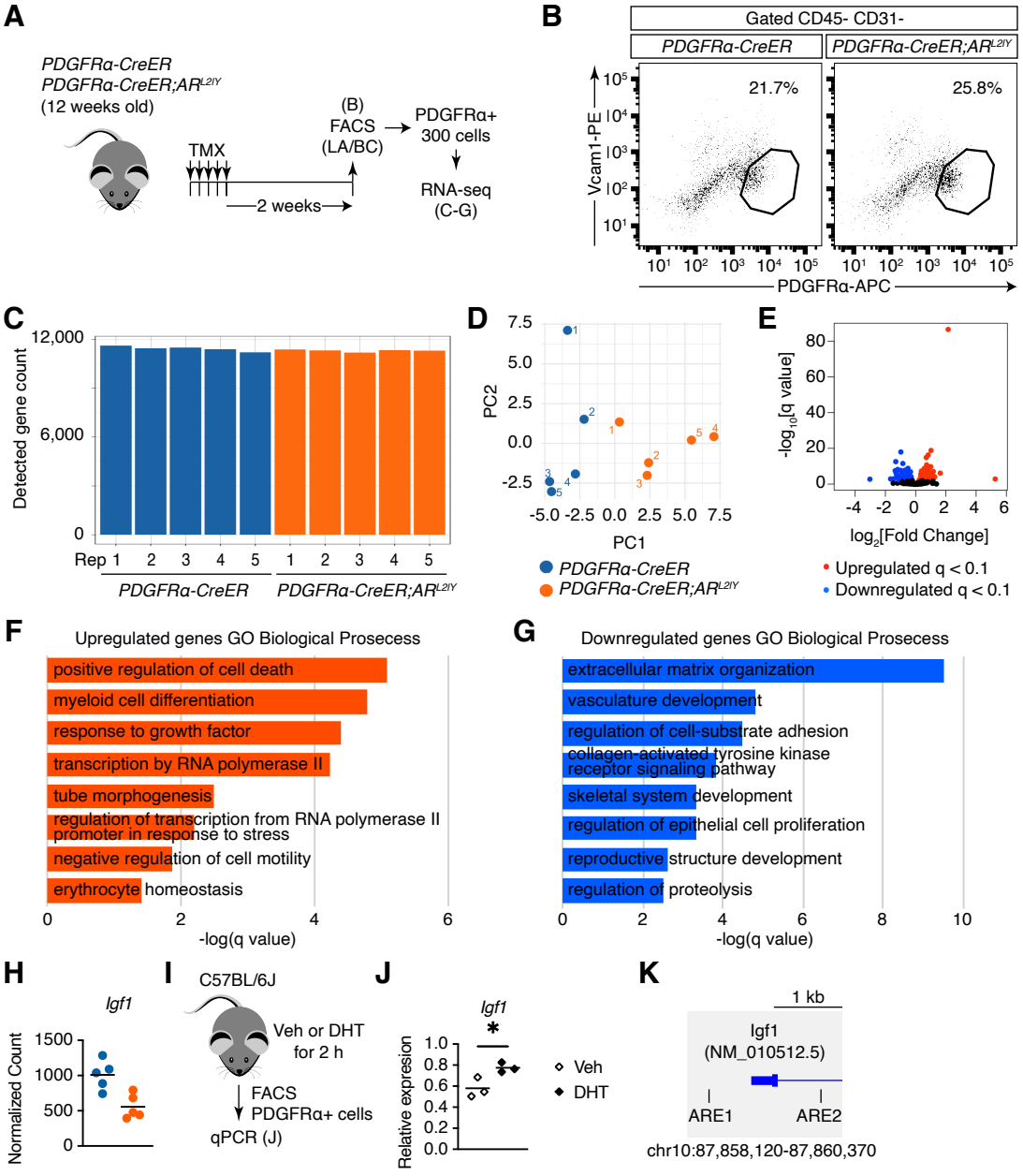

Figure 6 Sakai et al.